Linearized Free Surface URANS Approach for Ship Hydrodynamics

Vuko Vukčević, Inno Gatin and Hrvoje Jasak
University of Zagreb, Zagreb/Croatia, {vuko.vukcevic, inno.gatin hrvoje.jasak}@fsb.hr

1 Introduction

The Computational Fluid Dynamics represents an active and rapidly expanding area of research in ship hydrodynamics, where researchers have focused on resolving detailed physics that include the effects of: vorticity, viscosity, nonlinearity, free surface, turbulence, *etc.* (see [Larsson et al., 2015] for state–of–the–art CFD ship hydrodynamics simulations). Such high–fidelity simulations are extremely accurate and provide valuable insight on flow phenomena in research and industry, however, they still require significant computational resources for everyday industrial use.

A common simplification in early days of numerical ship hydrodynamics has been the linearization of the free surface boundary condition. The linearization can yield an efficient set of tools, however, most of them rely on potential flow theory with severely limited success to certain ship hydrodynamic flows. Recently, Wooliscroft and Maki [Woolliscroft and Maki, 2016] introduced a Reynolds Averaged Navier–Stokes (RANS) CFD model with linearised kinematic and dynamic free surface boundary conditions, in order to reduce the CPU time, while retaining the necessary accuracy required for manoeuvring predictions in the design phase of the ship. The method has been successfully applied to steady resistance and pure yaw predictions, where a significant speed–up compared to fully nonlinear and two–phase CFD methods.

This work presents an extension of the original linearised free surface model by Wooliscroft and Maki [Woolliscroft and Maki, 2016] in order to be able to calculate general seakeeping of a ship, including the wave–ship interaction. The mathematical and numerical models implemented in OpenFOAM are first briefly discussed, followed by preliminary results regarding: steady resistance, diffraction, seakeeping and manoeuvring with overset grids.

2 Mathematical and Numerical Modelling

The mathematical model of an incompressible, single–phase, turbulent flow with linearised free surface boundary conditions is presented, followed by details on the numerical model based on the arbitrary polyhedral Finite Volume (FV) method [Jasak, 1996] for pressure, velocity and turbulence and the Finite Area (FA) method [Tuković and Jasak, 2012] for surface elevation equation.

2.1 Mathematical Model

RANS governing equations for a single–phase, incompressible and turbulent flow read:

$$\nabla \cdot \mathbf{u} = 0\,, \quad \mathbf{x} \in \Omega\,, \tag{1}$$

$$\frac{\partial \mathbf{u}}{\partial t} + \nabla \cdot \Big((\mathbf{u} - \mathbf{u}_g)\mathbf{u}\Big) - \nabla \cdot (\nu_e \nabla \mathbf{u}) = -\frac{1}{\rho}\nabla p_d\,, \quad \mathbf{x} \in \Omega\,, \tag{2}$$

where $\mathbf{u}$ is the velocity field, $\mathbf{u}_g$ is the relative velocity due to the grid motion, ν_e is the effective kinematic viscosity, ρ is a constant fluid density and p_d is the dynamic pressure. Ω is the fluid domain, extending only up to calm free surface due to linearization of the free surface boundary conditions, while $\mathbf{x}$ is the radii vector. Effective viscosity ν_e is obtained by utilizing the $k - \omega\ SST$ model with standard wall functions. The gravitational acceleration is lumped inside the dynamic pressure using the following decomposition of pressure into hydrostatic and dynamic components:

$$p = p_d + \rho \mathbf{g} \cdot \mathbf{x}\,, \tag{3}$$

where $\mathbf{g}$ is the gravitational acceleration and $\mathbf{x}$.

In addition to RANS equations for the fluid flow, the free surface is described with a single–valued wave elevation function η with the following governing equation arising from kinematic boundary condition:

$$\frac{\partial \eta}{\partial t} + \nabla \cdot \Big(\mathbf{u}_{fs} - \mathbf{u}_{gfs}\Big)\eta = \mathbf{u}_{fs} \cdot n_{fs}\,, \quad \mathbf{x} \in \Gamma_0\,, \tag{4}$$

where $\mathbf{u}_{fs}$ is the velocity field at the free surface, $\mathbf{u}_{gfs}$ is the free surface velocity field due to possible grid motion and n_{fs} is the normal vector to the calm free surface Γ_0. As the free surface boundary condition is linearised [Woolliscroft and Maki, 2016], the calculated elevation defines the pressure boundary condition for the RANS flow field:

$$p = \rho|\mathbf{g}|\eta\,. \tag{5}$$

Hence, a direct coupling between velocity field $\mathbf{u}$, surface elevation field η and pressure field is present ($\mathbf{u} \rightarrow \eta \rightarrow p$).

Since the final goal of the model is to efficiently simulate seakeeping of a ship in mild waves, we introduce:

- Implicit relaxation zones [Jasak et al., 2015] for wave generation and absorption, where the momentum equation Eq. (2) and surface elevation equation Eq. (4) are blended with the corresponding relaxation equation based on a given wave theory (see Jasak *et al.* [Jasak et al., 2015] for additional details),
- Six Degrees–of–Freedom (6 DOF) rigid body motion equations.

2.2 Numerical Modelling

RANS equations, Eq. (1) and Eq. (2) are discretised with arbitrary polyhedral FV framework within foam–extend–4.0, a community driven fork of the open source software OpenFOAM [Weller et al., 1998]. The time derivative term is discretised using either first order accurate Euler implicit scheme for calm water resistance simulations or with second order accurate backward scheme for wave related simulations (wave diffraction and seakeeping). The convection term in the momentum equation is discretised with Guass' theorem using linear upwind interpolation while diffusion terms (in momentum and pressure equation) are also discretised with Gauss theorem using central differencing and over–relaxed approach to non–orthogonal correction [Demirdžić, 2015].

Free surface elevation equation, Eq. (4) is discretised directly at the boundary faces using the Finite Area (FA) approach [Tuković and Jasak, 2012] available in foam–extend–4.0. The time derivative term is discretised either with Euler or with backward scheme (for calm water resistance and wave simulations, respectively), while the convection term is discretised using second–order accurate linear upwind scheme.

A strong coupling between $\mathbf{u} \rightarrow \eta \rightarrow p$ is resolved using a segregated solution algorithm based on a combination of SIMPLE and PISO algorithms. The algorithm for a single time step is presented in 1. First, the 6 DOF equations are solved and the ship motion and the grid are updated. The surface elevation equation is solved next, followed by a momentum equation. The pressure equation is then formed and solved multiple times in order to converge the pressure–velocity–6 DOF fields without under–relaxation. Note that the enhanced coupling procedure as presented by Gatin *et al.* [Gatin et al., 2017] is used to update the rigid body motion equations after the solution of each pressure equation. The procedure is repeated until convergence.

Algorithm 1 Segregated solution algorithm for a time step.

```
while SIMPLE not converged do
    Update rigid body motion and move grid
    Solve surface elevation equation, Eq. (4)
    Solve momentum equation, Eq. (2)
    Update pressure boundary condition at the free surface, Eq. (5)
    while PISO not converged do
        Solve pressure equation, Eq. (1)
        Update rigid body motion
    end while
end while
```

3 Calm Water Resistance

Calm water resistance simulations for the Japan Bulk Carrier (JBC) [tok, 2015] is considered first. The model is $L_{PP} = 7$ meters long, at design speed corresponding to the Froude number $F_n = 0.142$ and is free to heave and pitch. Note that the present model is suitable for low Froude numbers due to linearised free surface boundary condition. Three grids are used to perform a grid convergence study:

- Coarse grid: 93 411 cells,
- Medium grid: 170 159 cells,
- Fine grid: 256 721 cells.

Details of the fine grid are presented in Figure 1. All grids extend: 1 L_{PP} in front of the ship, 1.5 L_{PP} after the ship, 1 L_{PP} towards the side and 1 L_{PP} towards the bottom. CFD results presented in Table 1 compare

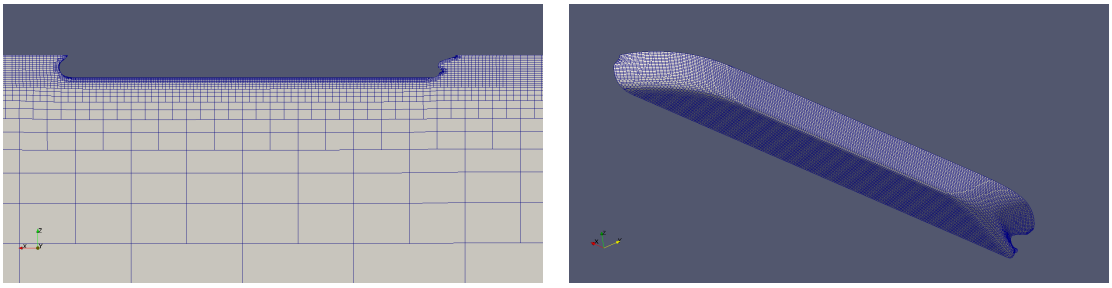

(a) Symmetry plane mesh.

(b) Hull surface mesh.

Fig. 1: Fine grid details (256 721 cells).

well with the available experimental data from the Tokyo 2015 Workshop [tok, 2015]. In addition, the frictional force is compared to the ITTC'57 correlation line, where it can be seen that the CFD results slightly under–predict the frictional resistance. The pressure force is lowered with grid refinement. Sinkage compares well with the experimental data, considering very small measured values ($\approx$ 6 millimetres). Furthermore, very small trim angle ($\approx 0.1^\circ$) is well predicted with the current model.

Overall, the results show good agreement with experiments considering the lower fidelity of the present model due to the linearisation of the free surface and coarse grids. The main benefit of the current model is the CPU time, where the simulation on fine grid took approximately four hours on four Intel Core i7-4820K @ 3.70GHz cores. The convergence of the total resistance for all three grids is presented

Table 1: Results for the calm water resistance for the JBC hull.

	EXP	**ITTC'57**	**GRID 1**	**GRID 2**	**GRID 3**
$C_F \times 10^3$	N/A	3.159	3.086	3.108	3.109
$C_P \times 10^3$	N/A	N/A	1.536	1.272	1.126
$C_T \times 10^3$	4.289	N/A	4.622	4.380	4.235
σ, $\%L_{PP}$	-0.086	N/A	-0.112	-0.109	-0.108
τ, $\%L_{PP}$	-0.180	N/A	-0.206	-0.192	-0.194

in Figure 2a, where the converged solution is reached at approximately $t = 70$s (after 7 000 iterations with $\Delta t = 0.01$ s). The convergence of sinkage for all grids is presented in Figure 2b.

4 KVLCC2 Wave Diffraction

In order to validate wave diffraction, a full scale KVLCC2 model is considered [tok, 2015] at zero forward speed. Five incident wave frequencies are considered: 0.2, 0.3, 0.4, 0.5 and 0.6 rad/s, while the

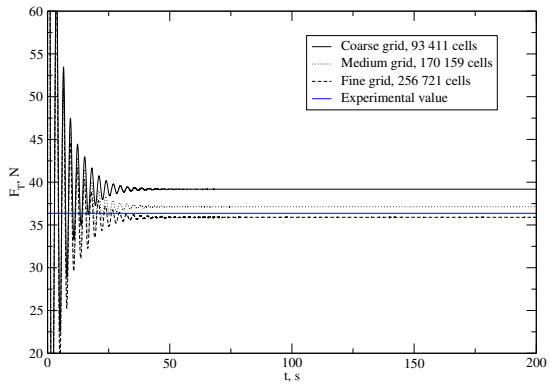

(a) Convergence of the total resistance.

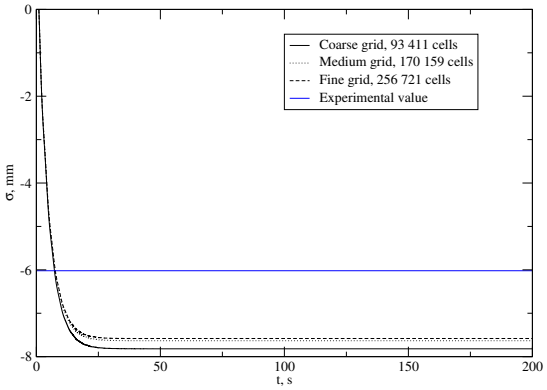

(b) Convergence of the sinkage.

Fig. 2: Convergence of CFD simulations using three grids.

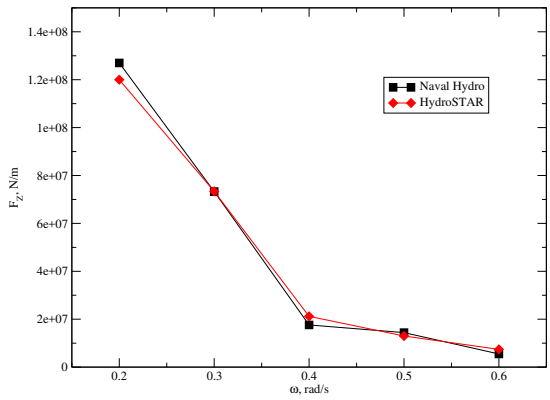

(a) First order amplitude of the heave force.

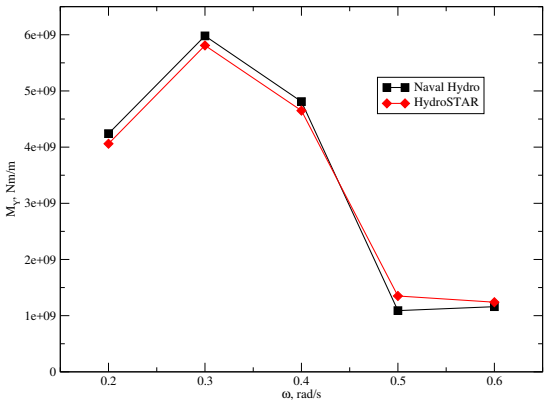

(b) First order amplitude of the pitch moment.

Fig. 3: First order amplitudes for KVLCC2 wave diffraction.

wave steepness is $ka = 0.05$, where k is the deep water wave number and a is the wave amplitude. Small steepness is used in order to remain within the validity region of linear free surface waves. A single mesh consisting of 800 000 cells is used for all wave frequencies.

The first order amplitude of the heave (vertical) force and pitch moment are presented in Figure 3a and Figure 3b, comparing well with the linearised, potential flow, frequency domain solver HydroStar. The first order phases for the same items are presented in Figure 4a and Figure 4b, both showing good agreement with HydroStar. It is important to note that the CFD simulations have been run for ten periods and the final solution is obtained by taking an average of the Moving Window FFT during last five periods.

5 KVLCC2 Seakeeping at Design Speed

Seakeeping simulations are performed for the KVLCC2 ship in model scale at design speed, with $L_{PP} = 3.2$ m (see [got, 2010] for details). Three cases are considered for the present study: $\lambda/L_{PP} = 0.5$, 1.1 and 2.0, where three grids are used correspondingly: 298K, 305K and 350K cells. Heave, pitch and mean value of resistance are compared to experimental data by Park *et al.*parkEtAl2015.

The comparison of heave and pitch first order amplitudes with the experimental data is presented in Figure 5a and Figure 5b. The CFD results compare well with experiments, except for the heave motion for $\lambda/L_{PP} = 2.0$, where the heave amplitude is higher than the theoretical limit $\eta/a = 1$ for long waves. This indicates that wave reflection occurred and needs to be investigated further.

The mean value of resistance is presented in Figure 6a, where it can be observed that the present results do not agree well with experiments. This is probably caused by the innate disability of the model

to take into account nonlinear effects such as added resistance in waves, or it might be related to post processing errors. Both possibilities shall be investigated in future. A perspective view of the free surface is presented in Figure 6b, indicating the ability of the model to take into account weakly nonlinear interaction between wave system generated by forward speed of the ship and incident, radiated and diffracted wave systems.

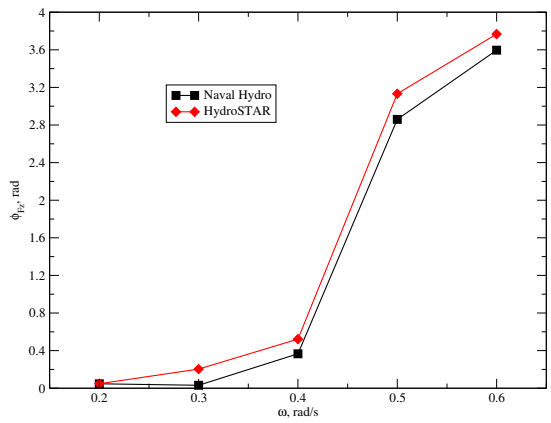

(a) First order phase of the heave force.

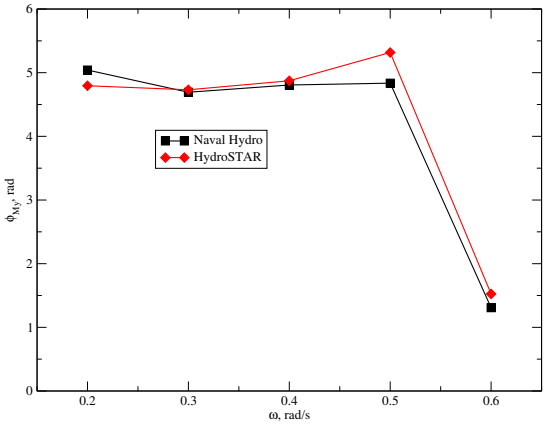

(b) First order phase of the pitch moment.

Fig. 4: First order phases for KVLCC2 wave diffraction.

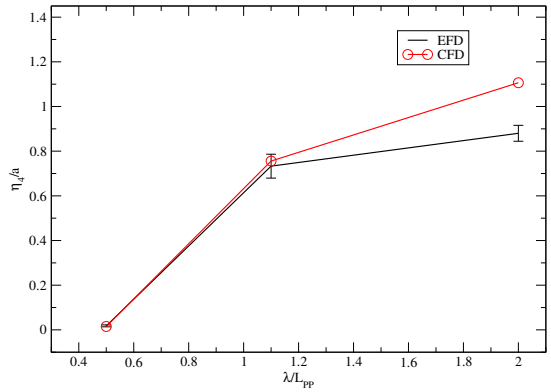

(a) First order heave amplitudes.

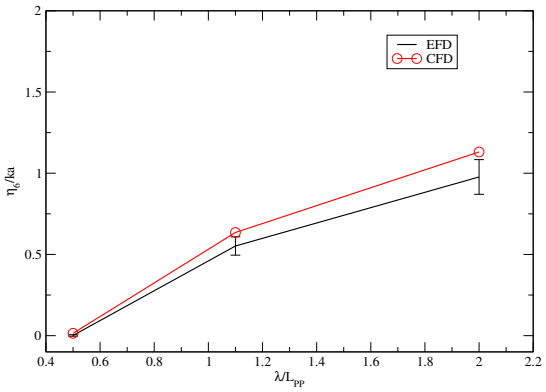

(b) First order pitch amplitudes.

Fig. 5: Comparison of first order motions for the KVLCC2 model.

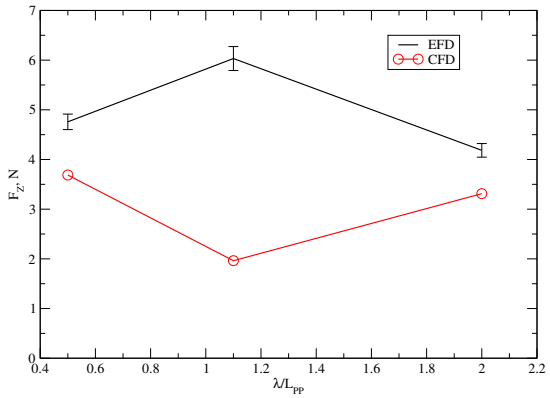

(a) Mean value of the total resistance.

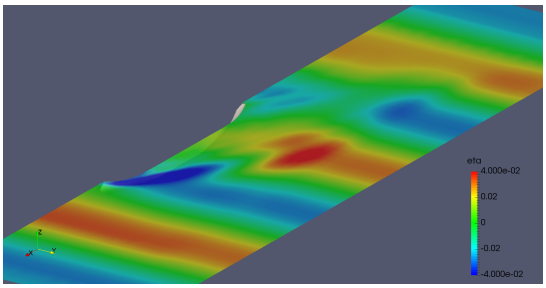

(b) Perspective view of the $\lambda/L_{PP} = 1.1$ simulation.

Fig. 6: Total resistance and free surface view for the KVLCC2 model.

6 Conclusion

This paper presents the linearised free surface URANS model for surface wave related problems such as wave diffraction and seakeeping of ships. The nonlinearity in the RANS equations is retained, while the free surface kinematic and dynamic boundary conditions are linearised, allowing us to consider single–phase flows without deforming the computational grid at the free surface.

The developed method is validated for calm water resistance and wave diffraction, showing good results compared to experiments and other numerical tools. The test cases indicate that the model is indeed suitable for cases where the free surface does not exhibit significant nonlinear behaviour (*i.e.* steep waves). The comparison of seakeeping tests with experimental data indicate the inability of the model to accurately predict the mean value of resistance in head waves at design speed. This problem shall be investigated further in future publications. Nevertheless, heave and pitch motions compare reasonably well with experiments.

The most important advantage of the model is its efficiency. Since the volume grid extends up to calm free surface, only part of the domain is meshed, thus saving the CPU time. All simulations have been carried out in parallel using four cores on a personal computer, which is hard to achieve with high–fidelity CFD models taking into account all the nonlinearities.

Acknowledgments

This research was sponsored by Bureau Veritas under the administration of Dr. Quentin Derbanne, whose technical and financial support is gratefully acknowledged.

References

(2010). Gothenburg 2010: A Workshop on CFD in Ship Hydrodynamics. `http://www.insean.cnr.it/sites/default/files/gothenburg2010/index.html`. [Online; accessed 20 August 2015].

(2015). Tokyo 2015: A Workshop on CFD in Ship Hydrodynamics. `http://www.t2015.nmri.go.jp/`. [Online; accessed 20 August 2015].

Demirdžić, I. (2015). On the Discretization of the Diffusion Term in Finite–Volume Continuum Mechanics. *Numer. Heat Transfer, Part B*, 68:1–10.

Gatin, I., Vukčević, V., Jasak, H., and Rusche, H. (2017). Enhanced Coupling of Solid Body Motion and Fluid Flow in Computational Fluid Dynamics. *Revised manuscript under review: Ocean Eng.*

Jasak, H. (1996). *Error Analysis and Estimation for the Finite Volume Method with Applications to Fluid Flows*. PhD thesis, Imperial College of Science, Technology & Medicine, London.

Jasak, H., Vukčević, V., and Gatin, I. (2015). Numerical Simulation of Wave Loads on Static Offshore Structures. In *CFD for Wind and Tidal Offshore Turbines*, pages 95–105. Springer Tracts in Mechanical Engineering.

Larsson, L., Stern, F., Visonneau, M., Hirata, N., Hino, T., and Kim, J., editors (2015). *Tokyo 2015: A Workshop on CFD in Ship Hydrodynamics*, volume 3, Tokyo, Japan. NMRI (National Maritime Research Institute).

Tuković, Z. and Jasak, H. (2012). A moving mesh finite volume interface tracking method for surface tension dominated interfacial fluid flow. *Comput. Fluids*, 55:70–84.

Weller, H. G., Tabor, G., Jasak, H., and Fureby, C. (1998). A tensorial approach to computational continuum mechanics using object oriented techniques. *Comput. Phys.*, 12:620–631.

Woolliscroft, M. O. and Maki, K. J. (2016). A fast-running CFD formulation for unsteady ship maneuvering performance prediction. *Ocean Eng.*, 117:154–162.